ELSEVIER

Chemical Engineering Journal 77 (2000) 165–177

Chemical Engineering Journal

www.elsevier.com/locate/cej

The catalytic combustion of natural gas in a membrane reactor with separate feed of reactants

H.W.J.P. Neomagus [a], G. Saracco [b], H.F.W. Wessel [a], G.F. Versteeg [a,*]

[a] *Department of Chemical Engineering, University of Twente, P.O. Box 217, 7500 AE Enschede, The Netherlands*

[b] *Dipartimento di Scienza dei Materiali e Ingegneria Chimica, Politecnico di Torino, C.so Duca degli Abruzzi 24, 10129 Torino, Italy*

Received 31 March 1999; received in revised form 10 October 1999; accepted 23 October 1999

Abstract

This paper provides an experimental and modelling analysis of the performance of a membrane reactor with separate feed of reactants for the combustion of methane. In this reactor concept methane and air streams are fed at opposite sides of a Pt/γ-Al_2O_3-activated porous membrane which hosts their reaction. The effect of a number of operating parameters (temperature, methane feed concentration, pressure difference applied over the membrane, type and amount of catalyst deposited, time of operation) over the attainable conversion was assessed, while measuring any possible slip of unconverted methane to the air-feed side. The maximum specific heat power load which could be attained with the most active membrane in the absence of methane slip was approximately 15 kW m^{-2} with virtually no NO_x emissions. Such potential might perhaps be exceeded if a properly designed membrane is tailored on purpose. For this sake a model, based on differential heat and mass balances throughout the membrane thickness, proved to be a promising design tool, since it allowed proper accordance with the experimental data with a single fitting parameter (pre-exponential kinetic constant).

Keywords: Catalytic combustion; Membrane reactor; Reactants

1. Introduction

The combustion of natural gas plays an important role in the supply of energy for a number of industrial or domestic applications [1]. Nowadays, most of the natural gas is burned out in conventional burners based on diffusive flames, where the gas is fed through nozzles to combustion chambers and meets the combustion air in flames where the temperature is generally well above 1000°C. Such high temperatures lead to undesired formation of NO_x whose emissions are regulated by more and more severe limits. The use of porous barriers, either catalytic [2] or non-catalytic [3], to host the combustion of methane is a promising tool to lower NO_x emissions. The solid matrix, made of high-temperature-resistant ceramics (e.g. mullite foams) or metals (e.g. Fe–Cr–Al alloy fibre mats [4]) gets hot owing to the heat provided by the combustion and radiates this heat out of the burner towards the heat sink. Since radiation is a much more effective heat transfer mechanism than convection, the major heat exchange route in the case of diffusive-flame burners, the combustion temperature might be kept at low values (700–1000°C), thereby lowering the NO_x outlet concentrations.

Most studies recently performed in this field were focused on pre-mixed burners, where a mixture of methane and combustion air (in reasonable excess: 10–30%) is fed to a thin porous burners (2–4 mm), which can confine the reaction front in its structure up to specific power inputs of 600–800 kW m^{-2}. Beyond these values, the momentum of the feed gas mixture starts to blow blue flames out of the burnerdeck, which reduces the above-mentioned advantages in terms of low-NO_x emissions.

The major drawback of fully premixed methane combustors lies in the fact that the feed air/methane mixture is highly explosive, which entails major safety problems, whose solution is accomplished through expensive flame-control instrumentation. Further, it is well known that the handling of catalytic combustion in conventional fixed-bed reactors might generate severe problems like thermal runaways, eventually leading to catalyst sintering [5].

A possible way to exploit the positive features of hosting the combustion inside a porous barrier and avoiding the underlined safety problems of pre-mixing, lies in the separate feed of methane and air at opposite sides of the mentioned barrier. In their pioneering studies, Trimm and Lam

* Corresponding author. Tel.: +31-53-489-4337; fax: +31-53-489-4774.
E-mail address: g.f.versteeg@ct.utwente.nl (G.F. Versteeg).

1385-8947/00/$ – see front matter
PII: S1385-8947(99)00163-1

[6] reported about such a reactor, in which methane and air diffuse in a fibre mat from opposite sides, and react onto a noble-metal catalyst.

A similar reactor concept has been developed at the University of Twente by van Swaaij and co-workers during the last decade. The reactants are introduced separately at opposite sides of a porous catalytic membrane, which is permeated by them and hosts their reaction. The first studies with this type of reactor were reported in literature by Sloot et al. [7] where it was demonstrated, using the Claus reaction as model reaction, that this concept has distinct advantages in the operation of reactions that normally require strict stoichiometric feed rates of reactants. Another application was worked out by Veldsink et al. [8] and Saracco et al. [9–11] for performing fast and exothermic reactions (in their studies: the catalytic combustion of CO and propane, respectively).

The most distinctive feature of this reactor compared with that by Trimm and Lam [6] lies in the much smaller pore size (ranging from 0.1 to 1 mm) of the porous alumina membranes employed, corresponding the so-called Knudsen–Poiseuille transition transport regime. This, on the one hand, reduces the attainable conversions per unit membrane surface, but, on the other hand, allows: (i) to reduce slips of reactants to opposite membrane sides (provided reaction kinetics are high enough); (ii) to achieve good flexibility and easy controllability (any change in reactant partial pressures in the gas feeds leads just to a shift of the reaction zone inside the membrane); (iii) to play upon the pressure difference between opposite membrane sides so as to promote a convective trans-membrane flow and to achieve a desired conversion level [10]. Further, when such a pressure difference is applied, an increase of the yield of intermediate products of a series of consecutive reactions could be reached because the convective flux generated would reduce the residence time of the intermediate products (recovered at the low pressure side) in the catalytic membrane [12].

The present work presents an extension of earlier studies on the catalytic combustion of propane to methane combustion, in order to check the potential of this reactor for heat production purposes. The effect of a number of operating parameters (temperature, reactants concentration, pressure difference applied over the membrane, etc.) over the achievable conversion and the completeness of the combustion process (slip of reactants throughout the membrane) has been assessed. For the sake of data interpretation, the high temperature level and the high heat generation rates compared to previous studies, required the upgrading of former isothermal models developed by Saracco et al. [9,10], by the inclusion of heat balances inside the membrane. In fact, local temperature gradients can play a role on the achievable conversions, and the constitutive parameters used in the model (e.g. diffusivities, viscosity) are usually dependent on the temperature. A second implication of the occurrence of high temperatures inside the membrane, can be the enhanced deactivation of the catalyst. Therefore, special attention was also paid, in line with the work of Saracco et al. [11], to the role played by the amount, distribution and long-term stability of the catalyst inside the membrane.

2. Theory

In earlier papers concerning the operation and the modelling of membrane reactors with separate feed of reactants it was demonstrated that the use of a Stefan–Maxwell approach, particularly in the presence of a pressure difference over the membrane, has to be preferred to a merely Fickian approach [7,8,10]. In this context, the so-called Dusty-Gas Model approach [13] was successfully employed in models based on membrane isothermicity, an assumption supported by the comparatively high membrane conductivity and the limited conversions tested in the above studies. In the present work, the high temperature level of the experiments carried out and the occasional presence of temperature differences measured between opposite membrane sides forced us to include trans-membrane heat balances in a new model set-up. With reference to the cylindrical coordinates system fitting the membrane shape (Fig. 1) the mass balance for a generic component i inside the membrane becomes

$$\frac{\varepsilon}{\mathrm{R}}\frac{\partial(p_i/T)}{\partial t} = -\frac{1}{r}\frac{\partial(rN_i)}{\partial r} + R_i, \tag{1}$$

whereas the corresponding heat balance is

$$\frac{\partial(\rho_{\mathrm{m}}c_{\mathrm{p,m}}T)}{\partial t} = -\frac{1}{r}\frac{\partial(Qr)}{\partial r} + \frac{R_i}{\nu_i}(-\Delta H^0), \tag{2}$$

where the enthalpy of reaction was set equal to 800 kJ mol^{-1}.

This set of equations is completed by a simple mole-fraction-consistence relationship

$$\sum p_i = \sum y_i P = P. \tag{3}$$

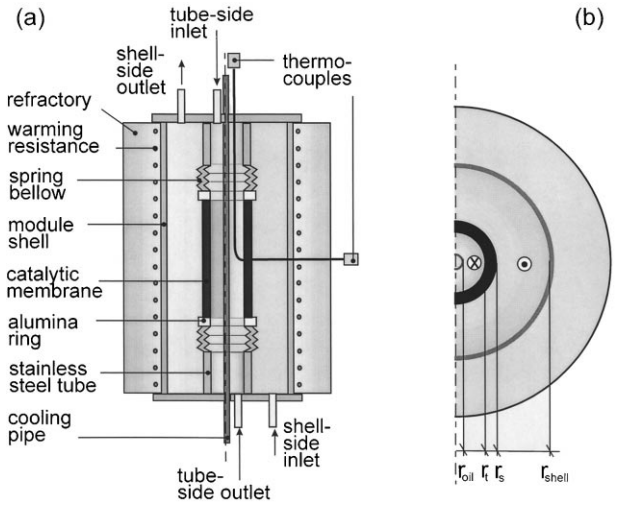

Fig. 1. Schematic representation of the catalytic membrane reactor: (a)=axial-section; (b)=cross-section.

Partial pressures (p_i) and/or mole fractions (y_i) in the bulk of the tube- or the shell-side were evaluated as logarithmic means of the inlet and outlet values, assuming a plug-flow regime at both membrane sides. This assumption was proven to be quite satisfactory by Saracco et al. [9].

Constitutive equations of mass and heat fluxes are provided by Stephan–Maxwell and Fourier laws, respectively

$$\sum_{j=1,j\neq i}^{n}\frac{y_iN_j-y_jN_i}{D^{\mathrm{e}}_{ij}}-\frac{N_i}{D^{\mathrm{e}}_{i,\mathrm{k}}} = \frac{P}{\mathrm{R}T}\frac{\partial y_i}{\partial r}+\frac{y_i}{\mathrm{R}T}\left(\frac{B_0P}{\mu D^{\mathrm{e}}_{i,\mathrm{k}}}+1\right)\frac{\partial P}{\partial r}; \quad (4)$$

$$Q=-\lambda^{\mathrm{e}}\frac{\partial T}{\partial r}. \quad (5)$$

Conversely, as concerns reaction kinetics, the following expression was adopted, in line with Spivey [14]:

$$R_i=\nu_i k_{\mathrm{r}}\frac{p_{\mathrm{CH_4}}}{\mathrm{R}T}, \quad (6)$$

where

$$k_{\mathrm{r}}=k^{\mathrm{o}}_{\mathrm{r}}\exp\left(-\frac{E_{\mathrm{a}}}{\mathrm{R}T}\right) \quad (7)$$

where the reaction coefficients are those of the complete combustion reaction

$$\mathrm{CH_4}+2\mathrm{O_2}\rightarrow\mathrm{CO_2}+2\mathrm{H_2O}. \quad (8)$$

At the membrane inner (tube-side) [15] and outer (shell-side) boundaries the following conditions were set for mass and heat transfer, respectively:

$$r=r_{\mathrm{t}}: \quad 1+\frac{y_i(t,r_{\mathrm{t}})-\langle y_i\rangle_{\mathrm{t}}}{\left(N_i(t,r_{\mathrm{t}})/\sum_{j=1}^{n}N_j(t,r_{\mathrm{t}})\right)-y_i(t,r_{\mathrm{t}})} = \exp\left(-\frac{\mathrm{R}T\sum_{j=1}^{n}N_j(t,r_{\mathrm{t}})}{P(k_{\mathrm{g}i})_{\mathrm{t}}}\right) \quad \text{(Bird et al. [15])}; \quad (9)$$

$$T=T_{\mathrm{t}} \quad \text{(experimentally measured value)}; \quad (10)$$

$$r=r_{\mathrm{s}}: \quad 1+\frac{y_i(t,r_{\mathrm{s}})-\langle y_i\rangle_{\mathrm{s}}}{\left(N_i(t,r_{\mathrm{s}})/\sum_{j=1}^{n}N_j(t,r_{\mathrm{s}})\right)-y_i(t,r_{\mathrm{s}})} = \exp\left(-\frac{\mathrm{R}T\sum_{j=1}^{n}N_j(t,r_{\mathrm{s}})}{P(k_{\mathrm{g}i})_{\mathrm{s}}}\right); \quad (11)$$

$$T=T_{\mathrm{s}} \quad \text{(experimentally measured value)}. \quad (12)$$

Shifting finally to the constitutive parameters (diffusivities, heat conductivities, etc.) they were either measured or estimated as follows:

- K_0, B_0: the Knudsen and Darcy coefficients of the membrane were determined experimentally through permeation experiments with inert gases, as indicated by Saracco et al. [9];
- $D^{\mathrm{e}}_{i,\mathrm{k}}$: the effective Knudsen diffusion coefficient was evaluated through the typical expression

$$D^{\mathrm{e}}_{i,\mathrm{k}}=\frac{4}{3}K_0\sqrt{\frac{8\mathrm{R}T}{\pi M_i}}. \quad (13)$$

- D^{e}_{ij}: the effective bulk diffusion coefficient was evaluated as $D^{\mathrm{e}}_{ij}=(\varepsilon/\tau)D^{\mathrm{o}}_{ij}$, where the binary diffusion coefficients were determined through the Füller–Schettler–Giddings equation [16], ε can be measured by Hg-porosimetry, whereas τ was determined through experiments carried out under operating conditions in which conversion was completely controlled by transport of reactants, as detailed in the next section.
- λ^{e}: the effective heat conduction coefficient was evaluated as a function of its conductive and convective contributions through the following expressions [17]:

$$\lambda^{\mathrm{e}}=(\lambda^{\mathrm{e}})_{\mathrm{cond}}+(\lambda^{\mathrm{e}})_{\mathrm{conv}}; \quad (14)$$

$$\frac{(\lambda^{\mathrm{e}})_{\mathrm{cond}}}{\lambda^{\mathrm{o}}}=\frac{\varepsilon}{1.5}+\frac{1-\varepsilon}{0.312(\varepsilon)^{2.32}+(2/3)(\lambda^{\mathrm{o}}/\lambda^{\mathrm{s}})}; \quad (15)$$

$$Pe=-2\frac{B_0}{\mu}\frac{\partial P}{\partial r}\frac{\rho^{\mathrm{o}}c^{\mathrm{o}}_{\mathrm{p}}r_{\mathrm{p}}}{(\lambda^{\mathrm{e}})_{\mathrm{conv}}}, \quad (16)$$

where the Peclet number was taken equal to 1.7 as suggested by these last authors, the solid-phase heat conductivity (λ^{s}) was experimentally measured as detailed in the following section, and the gas-phase conductivity (λ^{o}) evaluated, as the viscosity, through Chung-type relationships [16]. Finally, $c^{\mathrm{o}}_{\mathrm{p}}$ was calculated as a function of temperature through the contribution method also reported by Reid et al. [16].

- $(k_{\mathrm{g}i})_{\mathrm{t}}$, $(k_{\mathrm{g}i})_{\mathrm{s}}$: the external mass transfer coefficients at the shell and at the tube-sides of the membrane were evaluated, as already mentioned in [9], on the basis of the Chilton–Colburn analogy and of the work of Lundberg et al. [18], who solved the problem of heat transfer in laminar regime across annular passages between walls having different temperatures

$$(k_{\mathrm{g}i})_{\mathrm{s}}=2.63\frac{D^{\mathrm{o}}_i}{r_{\mathrm{shell}}-r_{\mathrm{s}}}, \quad (17)$$

$$(k_{\mathrm{g}i})_{\mathrm{t}}=1.73\frac{D^{\mathrm{o}}_i}{r_{\mathrm{t}}-r_{\mathrm{oil}}}, \quad (18)$$

where the diffusion coefficient in the gas phase of each chamber $\mathrm{D}^{\mathrm{o}}_i$ can be acceptably approximated by the bulk diffusion coefficients of the component i in pure nitrogen, calculated via the mentioned Füller–Schettler–Giddings equation.

- k^{o}, E_{a}: shifting finally to kinetics parameters, E_{a} was estimated by a kinetic study detailed in the next section, whereas k^{o} was left as the only fitting parameter of the model.

By setting proper initial profiles through the membrane of each of the seven variables (temperature, pressure and 5 mol

fractions: methane, oxygen, carbon dioxide, water and nitrogen), the above set of partial differential equations was solved through a tailor-made code based on the finite difference method, running through the Delphi 3 (Borland) platform on a PC.

3. Experimental

3.1. Catalytic membrane preparation

Some tubular α-alumina porous membranes (length=100 mm; inside diameter=14 mm; outside diameter=20 mm) were purchased from Velterop BV (Heerhugowaard, The Netherlands). The nominal pore size range (0.7 μm) was chosen so as to get well inside the transition regime between Knudsen and Poiseuille flow types. Two membranes were then activated through the following route:

1. γ-Al_2O_3 was precipitated in the pores of the membrane to provide a suitable specific surface area for supporting the catalyst. The following steps were accomplished for this purpose [19]:
   - an $Al(NO_3)_3{\cdot}9H_2O$ (400 g l^{-1})+urea (250 g l^{-1}) aqueous solution was prepared at 50°C to enable rapid dissolution of the precursors;
   - the membrane was impregnated with such solution under vacuum (so as to eliminate the gases trapped inside the membrane pores) and kept overnight at 95°C in closed vessels in order to promote urea hydrolysis and consequent $Al(OH)_3$ precipitation;
   - the membrane underwent then the following heat treatment: drying at 105°C for 4 h; heating up to 230°C at a 2°C min^{-1} rate; 1 h stay at 230°C (a massive production of gases takes place from the decomposition of precursors); heating up at 700°C at a 2°C min^{-1} rate; 4 h stay at 700°C; cooling down to room temperature at a 2°C min^{-1} rate.
2. Platinum was then deposited within the membranes by the incipient wetness impregnation method, using a H_2PtCl_6 aqueous solution as the precursor [20]. The H_2PtCl_6 precursor concentration was then tuned so as to synthesise in a single deposition the desired platinum content. After calcination for 2 h at 700°C in calm air, the Pt was then reduced for 12 h under H_2 flow at a temperature of 400°C, chosen in accordance with the findings of Barbier et al. [21].

A first membrane was prepared, named hereafter 'Membrane 1', with 4 wt.% γ-Al_2O_3 content and a Pt weight concentration, referred to the deposited γ-Al_2O_3, equal to 1% (a typical value for industrial Pt/γ-Al_2O_3 catalysts).

A second membrane was then prepared, named hereafter 'Membrane 2', with a lower γ-Al_2O_3 content (3 wt.%) so as to enable higher membrane permeability, and an enhanced Pt concentration 7 wt.% (once again referred to the γ-Al_2O_3) in order to possibly increase the reaction kinetics and to be able to achieve higher methane conversions per unit membrane area.

Twin membranes were prepared in both cases, following identical preparation routes, so as to perform destructive analyses such as mercury porosimetry or SEM-EDAX observation of Pt distribution inside the membrane.

3.2. The pilot plant

The catalytic membrane reactor is schematically represented in Fig. 1. Inside the ceramic tube a concentric cooling-oil pipe (inner diameter=3.80 mm, outer diameter=5.95 mm) is placed to remove the heat generated by combustion. A new membrane sealing technique, developed at the University of Twente was applied, which permits examination of the reactor performance up to a temperature of nearly 1000 K (200 K higher than previous techniques used in the earlier studies on propane oxidation [9]): the membrane is joined through a ceramic sealant to alumina rings, over which, through a multiple brazing technique, stainless steel tubes provided with spring bellows were sealed. The presence of such bellows allows us to eliminate thermally induced stresses along the axial coordinate. The catalytic membrane was placed in a stainless steel module (internal diameter=50 mm) surrounded by a PID-regulated electrical oven for thermal control and start-up purposes. Among others, two thermocouples (all of the K-type) were touching the surface of the membrane to possibly measure temperature differences over the membrane. One thermocouple was entering the reaction module along the oil pipe and touched the tube-side membrane surface at the middle of its axial length, whereas the other thermocouple was located at the same axial position but touching the shell-side membrane surface (see Fig. 1). The experiments were carried out at two temperature levels (average of the two thermocouple measurements): 823 and 973 K.

The absolute pressures at the tube and the shell-side were controlled in the range 1.5–2.5 bar (maximum pressure difference between opposite membrane sides: 1 bar), via Tescom back pressure regulators and monitored via Druck pressure transducers. In a single series of runs (dead-end experiments) the outlet of the methane feed side was closed, thereby forcing the entire methane feed flow rate to permeate the membrane. In such cases, the equilibrium pressure reached at the methane feed side was, of course, a function of the feed flow rate.

The feed gases (methane, air, nitrogen, by Hoekloos) were dosed through Brooks mass flow controllers. By these means the methane feed concentration at the one membrane side could be varied between 0.1 and 1, whereas pure air was fed at the opposite membrane side in any run performed. Inlet and outlet gas compositions are analysed using a Varian 3300 gas chromatograph fitted with a HayeSep column and both a TCD and a FID detector. Conversely, the CO_2 concentration was measured through a Maihak UNOR6N

Table 1
Structural characteristics of the tested membranes

	γ-Al_2O_3 (wt.%)	Pt (wt.%)	B_0 (m^2)	K_0 (m)	ε	τ
Membrane 1	4	0.04	8.1×10^{-16}	8.1×10^{-9}	0.346	4.85
Membrane 2	3	0.28	9.7×10^{-16}	9.2×10^{-9}	0.354	2.72

IR spectrometer. By these means overall mass balances of each component could be verified with deviations always less than 15%. No nitrogen oxides were ever detected in the effluent gases of the membrane reactors, a direct consequence of the comparatively low operating temperatures allowed by catalytic combustion.

3.3. Catalytic membrane characterisation

The prepared membrane underwent a series of either destructive (accomplished, as earlier detailed, on twin membranes prepared on purpose) or non-destructive analyses so as to measure structural (porosity, tortuosity, permeability) and other constitutive parameters necessary for modelling purposes (thermal conductivity, activation energy). Table 1 shows the prevalent structural parameters measured for both membranes.

In particular, the Darcy and Knudsen coefficients of each membrane were determined through inert gas permeation runs according to the procedures carefully described by Saracco et al. [9], and therefore not detailed here for the sake of briefness. Conversely, mercury porosimetry (Porosimeter 2000 — Carlo Erba Instruments) was used to measure the membrane porosity. Further, Pt concentration maps could be obtained on some membrane cross-sections by means of a SEM-EDAX microscope (Philips 525 M-EDAX 9100) so as to check whether the active species were evenly distributed inside the membrane or not. Fig. 2 reports, for instance, a Pt-distribution map determined on a cross-section of Membrane 1. Similar maps could be derived for other cross-sections of Membrane 1. Conversely, platinum was found to be much more evenly distributed inside Membrane 2.

Some other parameters, such as the membrane density and specific heat (used by the model in the accumulation term of the heat balance) were provided by the supplier as $2400\,kg\,m^{-3}$ and $1250\,J\,kg^{-1}\,K^{-1}$, respectively. Finally, the determination of three parameters (namely the heat conductivity, the tortuosity and the activation energy) required the use of tailored techniques described in the following sections.

3.3.1. Determination of λ^s

The heat conductivity of pure, crystalline materials can be expressed as follows [22]:

$$\lambda^s = \frac{a}{T} + b. \tag{19}$$

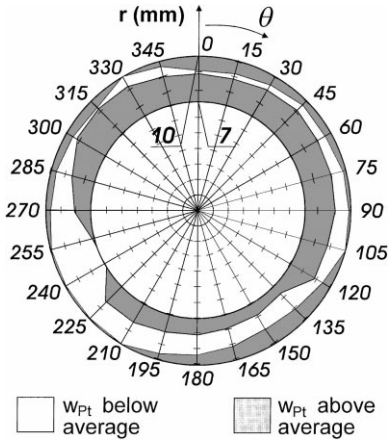

Fig. 2. Map of Pt distribution obtained by SEM-EDAX analysis on a cross-section of a membrane which underwent the same catalyst deposition procedure of Membrane 1.

The heat conductivity of dense alumina disks (Degussit AL23, supplied by Friatec: purity=99.5%; density=3800 $kg\,m^{-3}$; diameter=39 mm; thickness=5 mm) was measured in a tailor made apparatus, whose schematic representation is shown in Fig. 3. The sample is located between two reference blocks (stainless steel C-316; diameter=39 mm; thickness=30 mm) which are pressed between two heaters whose temperatures can be kept constant at desired values in the range (300–420 K). The sample, the reference blocks and the heaters are placed in a vessel, which is evacuated from air with a vacuum pump, to diminish heat losses by conduction and convection through the gas phase. Calibrated thermocouples (K-type, diameter=0.5 mm) are placed within both the sample and the reference blocks, via bored holes of

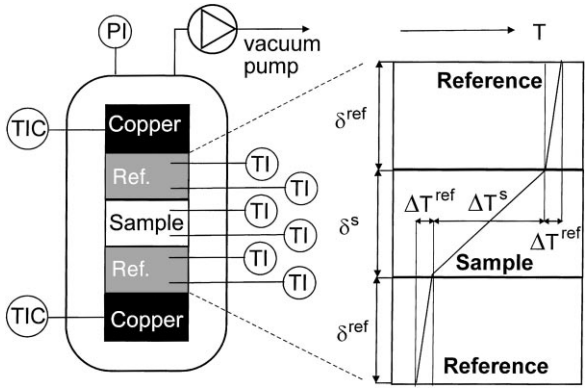

Fig. 3. Scheme of the experimental apparatus for the measurement of heat conductivity.

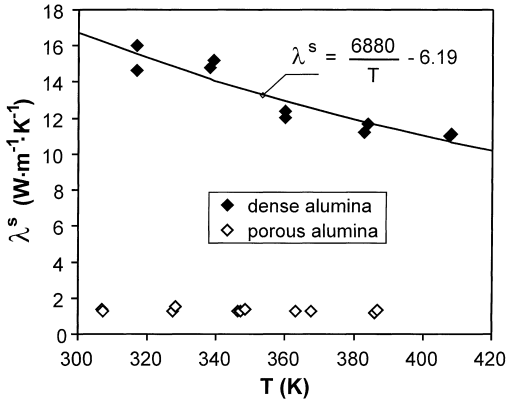

Fig. 4. Results of heat conductivity measurements on both dense and porous alumina disks.

approximately the same radius of the thermocouples. The measured temperatures are monitored continuously by a Philips PM 8237 multipoint data recorder, whereas the heat conductivity of the reference is taken from Peckner and Bernstein [23]

$$\lambda^{\mathrm{ref}} = 0.0135T + 12.663, \tag{20}$$

where the temperature is expressed in degree Celsius.

When a temperature difference is applied over the references, temperature profiles as those shown in Fig. 3 can be expected. If no heat losses occur from the sample and the references to the environment (which is hampered by the presence of vacuum), the heat conductivity of the sample can be easily calculated from

$$\lambda^{\mathrm{s}} = \lambda^{\mathrm{ref}} \frac{\Delta T^{\mathrm{ref}}}{\Delta T^{\mathrm{s}}} \frac{\delta^{\mathrm{s}}}{\delta^{\mathrm{ref}}}. \tag{21}$$

Since the heat conductivity is temperature dependent, ΔT^{s} was kept below 10°C during the measurements, so as to minimise errors. The results with dense alumina are depicted in Fig. 4, where the best-fitting line (Eq. (19): a=6880; b=−6.19) according to the least-squares method is drawn for dense alumina. The results obtained on alpha alumina porous disks (supplied by Velterop BV, ε=0.37; average pore diameter=0.1 μm; disk diameter=39 mm; thickness=4 mm) of the same characteristics of the virgin membrane tubes are reported as well.

If the above best-fitting equation is employed to predict λ^{s} at 823 and 973 K (the two temperature levels adopted in the experimental membrane-reactor runs), the values 2.17 and 0.88 W m^{-1} K^{-1} are derived, respectively.

3.3.2. Determination of E_{a}

Bulk Pt/γ-Al_2O_3 powders were prepared following as much as possible the same preparation conditions employed for the catalyst deposition inside the membranes (i.e. nitrate-urea route for the synthesis of the γ-Al_2O_3 support and incipient wetness impregnation with H_2PtCl_6 solutions, followed by 2 h-calcination at 700°C and 12 h-reduction with H_2 at 400°C, for the catalytic species Pt). The Pt content of the catalyst was 5 wt.%, an intermediate value between those characteristic of Pt/γ-Al_2O_3 catalysts deposited in Membrane 1 and in Membrane 2.

XRD analysis (PW1710 Philips diffractometer equipped with a monochromator on the diffracted beam Cu-Kα radiation) confirmed that the obtained catalyst-support powder was a transition alumina with a specific surface area of about 150 m^2 g^{-1}, determined by BET analysis (Sorptomatic Series 1800 — Carlo Erba Instruments). The BET surface area of the catalyst obtained after Pt-deposition was reduced by about 12% of that of the γ-Al_2O_3 support.

The catalyst powder was pressed by applying an absolute pressure of about 10^4 bar in order to form tablets, which were then crushed and sieved to select a specific particle-size range (0.2–0.5 mm), low enough to avoid significant internal mass transfer resistance in the kinetics-assessment experiments described below. The average internal void fraction of the prepared particles was about 43%, as measured by picnometry. 0.5 g of this granulated catalyst was placed in a quartz-tube micro-reactor for the assessment of reaction kinetics with special reference to the activation energy value.

The experimental apparatus used in the kinetic study was described in detail by Saracco et al. [24]. The plant is based on a continuous recycle micro-reactor, operated so as to render either external mass transfer resistance or the methane concentration gradient through out the fixed-bed of catalyst negligible. The recycle reactor was fed through a series of mass-flow controllers dosing gases from bottles (feed gas composition: CH_4=1–5%, O_2=20%, He=balance), whereas the analysis of the outlet gases was accomplished through a gas chromatograph (Hewlett Packard, mod. 5890 Series II, equipped with a Porapak QS column and a TCD sensor) and IR analyses (CO_2 analyser by Hartmann & Braun, mod. URAS 10E). Runs have been performed in the temperature range 550–750 K, whereas the absolute operating pressure was 1 bar. The kinetics expression used for data fitting was

$$R^*_{\mathrm{CH_4}} = \nu_i k^*_{\mathrm{r}} \frac{p_{\mathrm{CH_4}}}{\mathrm{R}T}, \tag{22}$$

where

$$k^*_{\mathrm{r}} = k^{*\mathrm{o}} \exp\left(-\frac{E_{\mathrm{a}}}{\mathrm{R}T}\right) \tag{23}$$

The experimentally determined $\ln(k^*_{\mathrm{r}})$ values are reported in Fig. 5 as a function of $1/T$. From the slope of the best fitting line (least-squares method) an activation energy value of 103 kJ mol^{-1} can be calculated.

3.3.3. Determination of τ

The value of the tortuosity of each membrane was determined through a series of reaction runs performed under completely-transport-controlled conditions (negligible slip of reactants through the membrane). Different methane concentrations (in the range 5–25 vol%) were

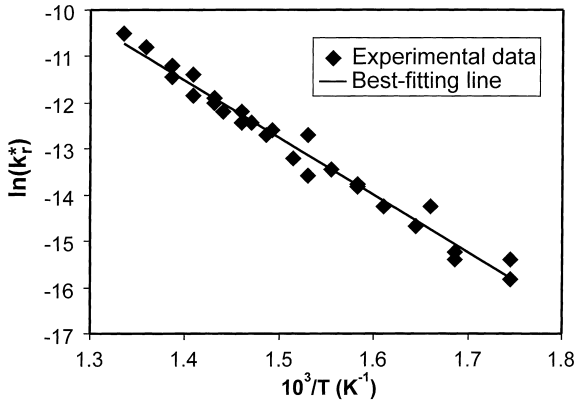

Fig. 5. Arrhenius plot of the kinetics data derived for methane combustion over the pelletised Pt/γ-Al_2O_3 catalyst (from the best fitting line: E_a=103 kJ mol^{-1}).

kept at the tube-side of the membranes (overall flow rate=32×10^{-6} Nm^3 s^{-1}), whereas pure air was fed at their shell-side (flow rate=32×10^{-6} Nm^3 s^{-1}), meanwhile maintaining 1.5 bar at both membrane sides. In these conditions, operating temperatures as high as 823 and 973 K had to be employed to meet the above transport-control constraint with Membranes 1 and 2, respectively. Under transport-controlled conditions, the kinetic constant could be set at a virtually infinite value and τ could be determined for each run as the only fitting parameter of the model. Fig. 6 shows the values of τ estimated through this procedure (least-squares fitting method) for both membranes as a function of the logarithmic-mean concentration of methane at the tube-side of the membrane.

The average estimates of the τ values of both membranes could thus be calculated as 4.85 and 2.72 for Membranes 1 and 2, respectively.

3.4. Membrane reactor runs

Several membrane reactor experiments were made in order to check the performance and the potential of the prepared catalytic membranes for methane combustion purposes in the separate feed reactor concept. The main goal of such experiments was therefore the measurement of the achievable methane conversion (i.e. specific heat power delivered) and of any possible slip of reactant (undesired since it reduces the advantages of the reactor concept here proposed) as a function of operating parameters such as membrane type, operating temperature, methane concentration, pressure difference applied over the membrane, etc. A few runs were also performed in a dead-end configuration, particularly amenable for practical application purposes, whereas a final ageing run was performed to enlighten the long-term stability of the catalytic membranes. The operating conditions and the main results obtained in each of the above series of runs are detailed in the paragraphs below.

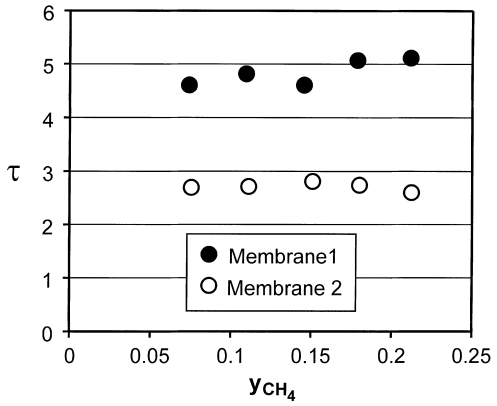

Fig. 6. Results of τ-estimation runs for both Membrane 1 (average τ value=4.85; operating temperature=973 K) and Membrane 2 (average τ value=2.72; operating temperature=823 K).

3.4.1. Isobaric experiments

The conversion of methane defined as

$$\zeta = \frac{\text{production rate of } CO_2 \text{ (mol s}^{-1})}{\text{methane feed rate in the reactor (mol s}^{-1})}, \quad (24)$$

as well as the slipped fraction of methane, defined as

$$S = \frac{\text{methane flow rate in the outlet stream of the shell-side (mol s}^{-1})}{\text{methane feed flow rate to the reactor (mol s}^{-1})} \quad (25)$$

were measured as a function of the methane concentration in the feed ($y^f_{CH_4}$=0.1–1), in the absence of a pressure difference over the membrane. During these experiments a constant methane stream (1.03×10^{-6} Nm^3 s^{-1} for Membrane 1 and 1.36×10^{-6} Nm^3 s^{-1} for the more active Membrane 2) was supplied to the tube-side of the reactor, while the concentration of methane was varied by changing the N_2 stream diluting the methane feed (the potential heat power of the gas stream was kept constant). A constant air stream was supplied to the shell-side of the membrane reactor (32×10^{-6} Nm^3 s^{-1}). The experiments were carried out with both membranes at 823 K (the measurement of the thermocouple touching the shell-side of the membrane was taken as a reference, whereas the value of the temperature measured over the tube-side surface was generally different by less than 5°C). Membrane 1 was also tested at 973 K, a temperature that was needed to achieve a transport controlled regime. The pressure on both sides of the membrane was 1.5 bar. Figs. 7 and 8 show the ζ and S values experimentally measured as a function of the methane inlet fraction for Membranes 1 and 2, respectively. Such figures show the best fitting model lines, as well. The k^o_r values determined by the least-squares fitting method were 3×10^7 and 170×10^7 s^{-1} for Membranes 1 and 2, respectively. Finally, Fig. 9 shows the concentration and temperature profiles inside Membrane 1, calculated by the model for two representative operating conditions indicated in Fig. 7.

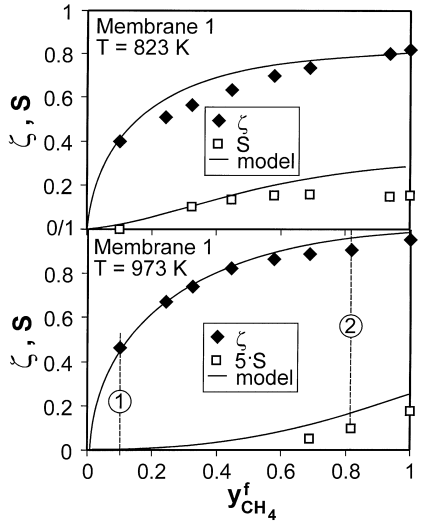

Fig. 7. Results of isobaric runs performed with Membrane 1 and comparison with model calculations. 1, 2=reference conditions for the concentration and temperature plots on Fig. 9.

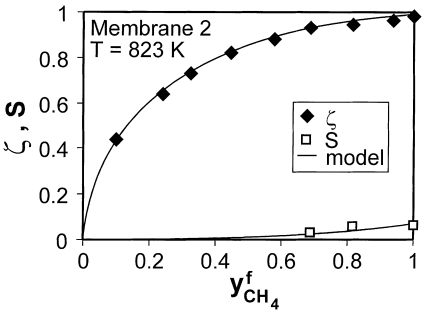

Fig. 8. Results of isobaric runs performed with Membrane 2 and comparison with model calculations.

3.4.2. Non-isobaric experiments and long-term stability test

Some experiments were carried out with both membranes in order to check the reactor operation with applied pressure differences over the membrane. The measurements were carried out at 973 K (Membrane 1) and 823 K (Membrane 2) and air was fed to the shell-side chamber of the reactor (32×10^{-6} Nm^3 s^{-1}), whereas a mixture of methane in nitrogen (y_{CH_4}=0.1) was fed to the tube-side one (15×10^{-6} Nm^3 s^{-1}). The pressure at the shell-side was kept constant at 1.5 bar, while the pressure at the tube-side varied from 1.5–2.5 bar.

In Fig. 10 the experimental total molar flow rate of methane converted (ϕ_c) in Membrane 1 and the flow rate of methane slipped to the shell-side of the membrane (ϕ_s) are plotted as a function of the applied pressure difference, together with model calculations based on the kinetic constant determined in the previous section. As far as Membrane 2 is concerned, Fig. 11 shows the equivalent experimental data obtained just after its preparation (fresh membrane) as well as those obtained after a long-term stability run (aged membrane), performed for 80 h at 823 K with no pressure

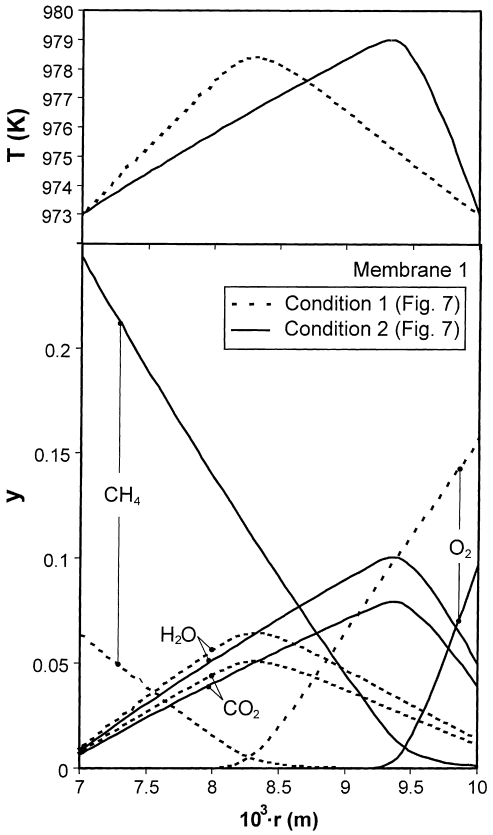

Fig. 9. Concentration and temperature profiles throughout Membrane 1 at 973 K, as calculated by the model for the reference conditions 1 and 2 of Fig. 7.

difference applied. No methane slip was noticed with the fresh membrane for any of the pressure differences applied.

Finally, a practical operation way of the catalytic membrane reactor with separated feed of reactants as a catalytic combustor is the so-called 'dead-end' mode. Therefore, dead-end experiments were carried out with pure methane fed at the tube-side ($0.8–2\times10^{-6}$ Nm^3 s^{-1}) and air at the shell-side of the more active Membrane 2. During these experiments the outlet of the tube was closed (dead-end) in order to direct the total gas flow through the membrane. The

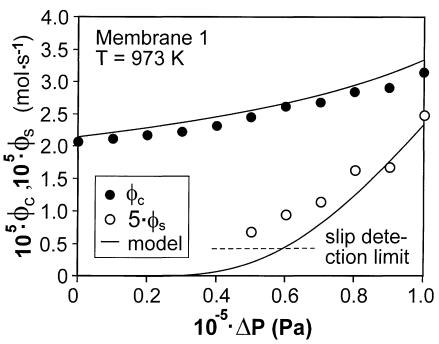

Fig. 10. Results of non-isobaric runs performed with Membrane 1 and comparison with model calculations.

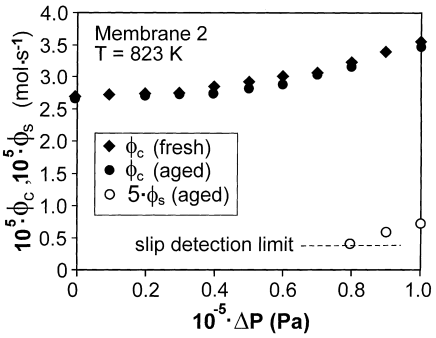

Fig. 11. Results of isobaric runs performed with Membrane 2 before and after the ageing treatment.

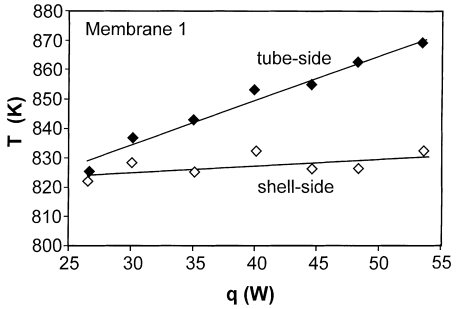

Fig. 12. Temperatures measured at opposite sides of Membrane 1 during the dead-end tests as a function of the heat flow rate generated by methane combustion.

ratio between the volumetric flows of methane and air was kept constant (0.055) during the experiments. The pressure at the shell-side was kept constant at 1.5 bar, whereas the pressure at the tube-side was 1.56–1.70 bar (depending on the methane flow). The temperature of the shell-side surface of the membrane was kept at 823 K. Methane conversion was approximately constant ($\zeta \approx 0.96$) for each run, whereas a certain slip of methane was always present (S=0.07–0.08). A distinctive feature observed during these dead-end measurements lies in more and more pronounced differences between the shell-side and the tube-side temperature measurements as long as the heat flow rate (q) generated by methane combustion was increased, as shown in Fig. 12.

4. Discussion

The results obtained in Section 3 are hereafter discussed following the order in which they were presented.

4.1. Membrane characterisation results

A first important issue related to the obtained membrane characterisation results lies in the uneven Pt distribution determined for Membrane 1 (Fig. 2). Particularly, the membrane zones closer to the external surfaces generally show a higher Pt catalyst content than the inner parts of it. It might be guessed if such behaviour is a direct consequence of: (a) some redistribution during the Pt deposition step, (b) equivalent uneven distribution problems arose during the previous γ-Al_2O_3 deposition step (by being selectively deposited onto the γ-Al_2O_3 support, the platinum should then suffer from the same misdistribution of this last phase). Based on previous studies on γ-Al_2O_3 deposition in porous structures through the nitrate urea method [25], hypothesis (b) is probably to be rejected, i.e. the transition alumina should not be preferentially located close to the membrane surface. On the grounds of the early studies by Maatman [26] and on the current industrial practice in the production of egg-shell catalysts, we are prone to think that as long as the Pt precursor solution enters the pores of the γ-Al_2O_3 deposited membrane it undergoes a rapid depletion of its concentration owing to strong adsorption of hexa-chloroplatinic ions over the γ-Al_2O_3 there present. As a consequence, the inner parts of the membrane will be reached by an impregnating solution with a diminished Pt-deposition potential and will result less rich of this catalytically active species [27]. Only when the H_2PtCl_6 solution is particularly concentrate it may lead to saturation the precursor chemisorption process occurring at the entrance of membrane pores, thereby allowing a deeper penetration of Pt and a more even distribution of it. This should be the main reason why Membrane 2, bearing a much higher Pt amount and a lower γ-Al_2O_3 loading than Membrane 1, did not show the Pt distribution problems of this last counterpart.

It must be stressed though that the non-uniform distribution of catalyst along the membrane thickness (r coordinate in Fig. 2) should not to be regarded necessarily as a defect. As a function of the operating conditions (i.e. reactants concentrations, pressure difference applied over the membrane) the reaction zone will move in a certain radial position (see Fig. 9). It should be thus advisable to provide a comparatively high catalyst concentration in the above location, leaving the remaining parts of the membrane active enough to cope with possible reaction-zone shifts originated by oscillations in the feed concentrations, flow rates and absolute pressures. Conversely, any depletion of the catalyst loading along the θ coordinate (Fig. 2) is in any case highly undesirable since it would favour local slips of methane. This should be particularly severe especially when the location of such Pt-poor zones is close to the air feed side since the slipping methane will not have chances of being reacted away in other Pt-rich zones of the membrane before leaving it. Unfortunately, an uneven distribution of Pt along θ seems to be a distinctive feature of Membrane 1, on which further parts of this discussion will be dedicated later on when commenting the results of the membrane reactor runs.

Shifting to the results of α-Al_2O_3 thermal conductivity measurements, a substantial agreement between the estimates drawn for λ^s at 823 and 973 K (2.17 and 0.88 W m^{-1} K^{-1}, respectively) can be found with the data reported by Itaya et al. [28] for the same material. However, if the data concerning dense and porous alumina are

considered (Fig. 4), as well as the simplified equation proposed by Loeb [29] to correlate such values (valid whenever radiation and pore orientation effects can be neglected)

$$\frac{\lambda^{p}}{\lambda^{s}} = 1 - \varepsilon, \tag{26}$$

a clear discrepancy between the λ^{p} values that can be calculated with Eq. (26) and those measured experimentally can be noticed, the latter being much lower than the former ones. A certain overestimation of the λ^{s} value of the actual membrane-constituting material can be hypothesised, possibly due to impurities or additives not declared by the membrane supplier. This point will be further addressed later on.

Conversely, as far as the activation energy value measured is considered, it must be observed that is perfectly in line with other estimates drawn by other researchers for Pt-based catalysts. For instance, Sicardi et al. [30] measured for methane combustion over Pt-Al_2O_3 catalysts with variable Pt content E_a values in the range 80–120 kJ mol^{-1}, whereas Anderson et al. [31] estimated for the same catalyst type an E_a value equal to 98.4 kJ mol^{-1}, quite close to the value determined in this work (103 kJ mol^{-1}).

Some final considerations go to the structural parameters evaluated for both membranes. The B_0, K_0, ε and τ obtained appear compatible with those found in previous studies on catalytic barriers activated through the nitrate-urea technique [9,10,32]. Further the higher B_0, K_0 and ε values obtained for Membrane 2 compared with those of Membrane 1 (Table 1) are an obvious consequence of the lower amount of catalyst deposited in Membrane 2 and confirm that this condition actually rendered this membrane more accessible to reactants than its counterpart. Similarly, the higher τ value calculated for Membrane 1 is possibly due to the highest chance of pore-blocking occurrence by the deposited catalyst due to the higher γ-Al_2O_3 loading of this membrane compared to Membrane 2. However, this mechanism might not be sufficient to justify such a sharp increase of τ (from 2.72 to 4.85), when the γ-Al_2O_3 concentration was varied from 3 to 4 wt.%. It is likely that the measured τ value lumps other effects, not well identified so far. In any case, owing to the way τ was measured (i.e. from reactive runs in completely-transport-controlled conditions), such lumping definitely improves the attitude of the model to predict properly the reactor performance.

4.2. Results of isobaric runs

A first consideration concerning the results of isobaric runs obtained with Membrane 1 is that the conversion of methane is strongly dependent on temperature (Fig. 7): conversion at 973 K is significantly higher than the conversion at 823 K. This observation indicates that the conversion rate of CH_4 is not completely mass transfer limited at this latter temperature. In the case of a complete mass transfer limited process, lower differences between conversions at different temperatures should be expected, due to the rather small activation energy of the diffusion coefficients. Conversely, when comparing the ζ values measured at 973 K for Membrane 1 with those obtained at 823 K with Membrane 2 (Fig. 8), quite comparable conversions are found for both cases. This observation, together with the rather low S values measured in these last conditions, is a strong indication in favour of a mass transfer limited process. The fact that Membrane 2 reaches such conditions at a much lower temperature than Membrane 1 and despite the methane feed flow rate is somewhat higher (1.36×10^{-6} Nm^3 s^{-1} and against the 1.03×10^{-6} Nm^3 s^{-1} used for Membrane 1), is a rather obvious consequence of its higher content of catalytically active element. By the way, as high heat power outputs as 15 kW m^{-2} can be approached with Membrane 2 with negligible slip of methane, a value in line with other separate-feed catalytic combustors mentioned in the Introduction [6], and that might be likely increased by a proper design of the catalytic membrane parameters accomplished through suitable modelling tool.

In fact, the comparison between the performance of the two membranes can be taken a step forward by considering the results of model calculations. In both cases, quite acceptable agreement between model predictions and experimental data can be observed for optimised values of the pre-exponential kinetic constant. However, the k_r^o values determined by the least-squares fitting method are quite far away from each other (Membrane 1: 3×10^7 s^{-1}; Membrane 2: 170×10^7 s^{-1}), much more than the different Pt content of the membrane should have suggested. In fact, the pre-exponential kinetic constant, often called frequency factor, should be proportional to the number of active sites per unit membrane volume, i.e. to the Pt content of the membrane, provided Pt is dispersed in clusters or particles of equal dimensions. A reasonable explanation for this issue might be found in the uneven catalyst distribution affecting, in particular, Membrane 1. It may be argued that, owing to the occurrence of slip of methane through Pt-poor regions, the k_r^o constant derived for Membrane 1 should have been markedly underestimated compared to its potential, membrane-averaged value. Similar effects cannot be excluded for Membrane 2, as well, but they should in any case be minor if compared with its less active counterpart due to the approximately even Pt distribution observed by SEM-EDAX analysis.

The possibility of slips through the membranes is maximised as long as the methane concentration is increased, thereby shifting the reaction zone towards the air-feed side (shell). Such shift of the reactor zone can be clearly noticed based on the concentration profiles plotted in Fig. 9, evaluated by the model according to the experimental conditions 1 and 2 indicated in Fig. 7 (Membrane 1 at 973 K, with methane feed mole fractions of 0.1 and 0.81, respectively). It is not surprising at all, then, that detectable S values appear for both membrane only for rather high methane feed concentration and increase when this last variable is increased. Further, following the above arguments concerning

the effect of Pt uneven distribution throughout Membrane 1, it might be guessed that the higher slip values observed for Membrane 1 compared with Membrane 2 are not only due to the lower platinum content, but also to the highly undesired presence of Pt-poor zones close to the shell-side membrane surface, where the reaction zone shifts for high $y^{f}_{CH_4}$ values.

Following earlier consideration of ours [10], the methane slipped to the air-feed side should have an additional chance of being catalytically converted by diffusing into dead-end pores of the membrane, originating from some pore-blocking by the deposited catalyst support, and accessible only from the shell-side of the membrane and therefore not interested by the trans-membrane fluxes of reactants. This effect, probably acquiring a certain importance only when rather high slips are taking place, is probably the main reason for the slight overestimation of the *S* value given by the model, which does not take into account the just-described mechanism, compared to the one actually measured through Membrane 1.

4.3. Results of non-isobaric runs and long-term stability test

Beyond the increase of methane concentration, another way to shift the reaction zone towards the air-feed side and to enhance the achievable conversion, is that of applying a pressure difference over the membrane, the high-pressure side being the methane-feed [10]. By these means a convective flow of methane is generated through the membrane and possibly converted, provided the reaction kinetics are high enough. This has been clearly confirmed by the data obtained in such operating conditions with both membranes (Figs. 10 and 11). Model calculations are once again in good agreement with experimental findings for Membrane 1 (Fig. 10). A similar accordance was observed for Membrane 2, as well. Moreover, for this last membrane no slip of methane was observed even for the highest pressure difference applied (1 bar), a sign of its superior activity in its 'as-prepared' form. Unfortunately, the long-term ageing treatment performed (continuous operation for 80 h at 823 K), turned out to deactivate slightly the membrane, leading to the presence of a slight methane slip molar rate (ϕ_s) at the highest applied pressure differences (>0.8 bar), the converted methane flow rate (ϕ_c) remaining rather constant (Fig. 11). This phenomenon, likely attributable to platinum particle agglomeration or to some collapse of the γ-Al_2O_3 surface area, suggests that, in case of any practical application of the present reactor concept, aged-catalyst conditions should be taken into account when designing the reactor so as to achieve an as constant as possible steady-state performance.

Coming finally to the dead-end experiments it should be admitted that to allow success of this rather simple and practical operation mode, thicker or more active membranes than Membrane 2 should be employed in order to eliminate the presence of slips. The use of thicker membranes may though increase the temperature gradients across it, thereby enhancing the risks of thermal deactivation of the catalysts. In this context, it has to be underlined that the temperature differences between the inner and outer surface of the membrane, measured above certain generated heat flow rates, are higher than those that can be expected on the basis of the model calculations (Fig. 9). A possible reason for this may lie in a certain overestimation of the thermal conductivity of the membrane. If the quite pronounced decrease of the thermal conductivity measured when shifting from dense alumina to porous alumina is considered (Fig. 4), it might be guessed that the method by Specchia and Sicardi [17] used for the evaluation λ^e, on the grounds of the only λ^s value of dense alumina (among other parameters), could perhaps provide higher-than-real effective thermal conductivity values. In any case, more precise temperature measurements than those attainable by thermocouples simply touching the external membrane surfaces should be employed to better elucidate this point.

5. Conclusions

A membrane reactor with separate feed of reactants was tested to assess its potential in the catalytic combustion of methane with air, getting confirmation of the numerous interesting properties enabled by this reactor when operating in the transport-controlled regime (high-enough temperature): (i) absence of slip (the reaction takes place entirely inside the membrane); (ii) easy controllability (flow rates, composition and pressure of each flow rate can be varied independently); (iii) thermal runaways are hampered (transport is much less temperature sensitive than kinetics); (iv) the pressure difference between opposite membrane sides can be used as a driving force to increase the overall conversion.

In view of a practical application of this reactor as a methane combustor for low-NO_x heat production purposes, it has to be once again underlined that the maximum specific heat power obtained in the present study, with negligible slip of methane to the air-feed side (an undesired occurrence which reduces the advantages of this membrane reactor), was close to 15 kW m^{-2} with the most active and permeable membrane employed (Membrane 2). This figure is perhaps too low (by at east one order of magnitude) if compared with those attainable with the less safe and versatile premixed catalytic burners (Saracco et al., 1999). As a consequence, a much wider membrane surface would be required, compared to this last burners, for a given heat power requirement. However, on the basis of the non-isothermal model presented and validated in this work, an optimisation of the structural parameters of the membrane (i.e. porosity, pore-size, catalyst amount, thickness, etc.) can be attempted, with the aim of designing a membrane reactor of maximised performance, possibly based on the dead-end configuration (more amenable to practical application).

A longer-term and perhaps even more interesting goal of this reactor concept, provided different catalysts than Pt/γ-Al_2O_3 are used, could be the production of synthesis gas by methane partial oxidation. In this context, the selectivity towards intermediate reaction products (CO and H_2) could be maximised through a proper use of the pressure difference applied over the membrane, so as to limit the residence time of such intermediates in the membrane itself [12].

6. Symbols

A	surface area (m^2)
B_0	permeability (m^2)
c_p	specific heat ($J\,kg^{-1}\,K^{-1}$)
D	diffusivity ($m^2\,s^{-1}$)
E_a	apparent activation energy ($J\,mol^{-1}$)
ΔH^0	standard heat of combustion ($J\,mol^{-1}$)
k_g	mass transfer coefficient ($m\,s^{-1}$)
k_r	kinetic constant referred to the membrane unit volume (s^{-1})
k_r^*	kinetic constant referred to the catalyst unit mass (s^{-1})
k_r^o	pre-exponential kinetic constant (s^{-1})
k_r^{*o}	pre-exponential kinetic constant ($m^3\,kg^{-1}\,s^{-1}$)
K_0	Knudsen coefficient (m)
M	molecular weight ($kg\,mol^{-1}$)
N	mole flux ($mol\,m^{-2}\,s^{-1}$)
p	partial pressure (Pa)
P	absolute pressure (Pa)
Pe	Peclet number
q	heat flow rate (W)
Q	heat flux ($W\,m^{-2}$)
r	radius (m)
R	ideal gas constant=8.314 $J\,mol^{-1}\,K^{-1}$
R	reaction term referred to the unit membrane volume ($mol\,m^{-3}\,s^{-1}$)
R^*	reaction term referred to the unit catalyst mass ($mol\,kg^{-1}\,s^{-1}$)
S	methane slip fraction
t	time (s)
T	temperature (K)
w	weight fraction
y	mole fraction
$\langle y \rangle$	*mixing-cup* mole fraction

Greek letters

δ	thickness (m)
ε	porosity
ϕ_c	molar flow rate of methane converted in the membrane reactor ($mol\,s^{-1}$)
ϕ_s	molar flow rate of methane slipped to the air feed side of the membrane reactor ($mol\,s^{-1}$)
μ	viscosity (Pa s)
ν	stoichiometric coefficient
θ	angular coordinate (°)
ρ	density ($kg\,m^{-3}$)
τ	tortuosity
ζ	per-pass conversion of methane throughout the membrane reactor

Subscripts

i, j	generic components
cond	conductive
conv	convective
exp	experimental
k	Knudsen
m	membrane
oil	cooling-oil pipe
s, t	shell-, tube-side of the catalytic membrane
shell	reactor module shell

Superscripts

e	effective
f	feed
o	gas phase
p	porous
ref	reference block
s	solid phase or sample

Acknowledgements

The financial support of Gastec is gratefully acknowledged.

References

[1] K.J.A. Hargreaves, H.R.N. Jones, D.B. Smith, Developments in burner technology and combustion science, in: 52nd Institution of Gas Engineers Autumn Meet., Vol. 1, London, 12 November 1986, p. 1309.
[2] G. Saracco, I. Cerri, V. Specchia, R. Accornero, Catalytic pre-mixed fibre burners for methane combustion, Chem. Eng. Sci., in press.
[3] D. Trimis, F. Durst, Combustion in a porous medium — advances and applications, Combust. Sci. Technol. 121 (1996) 153.
[4] B.A. Pint, A.J. Garratt-Reed, L.W. Hobbs, The reactive element effect in commercial ODS FeCrAl alloys, Mater. High Temp. 13(I) (1995) 3.
[5] G.F. Froment, K.B. Bishoff, Chemical Reactor Analysis and Design, Wiley, New York, 1979.
[6] D.L. Trimm, C.-W. Lam, The combustion of methane on platinum-alumina fibre catalysts II. Design and testing of a convective-diffusive type catalytic combustor, Chem. Eng. Sci. 35 (1980) 1731.
[7] H.J. Sloot, G.F. Versteeg, W.P.M. van Swaaij, A non-permselective membrane reactor for chemical processes normally requiring strict stoichiometric feed rates of reactants, Chem. Eng. Sci. 45 (1990) 2415.
[8] J.W. Veldsink, R.M.J. van Damme, G.F. Versteeg, W.P.M. van Swaaij, A catalytically active membrane reactor for fast, heterogeneous catalysed reactions, Chem. Eng. Sci. 47 (1992) 2939.

[9] G. Saracco, J.W. Veldsink, G.F. Versteeg, W.P.M. van Swaaij, Catalytic combustion of propane in a membrane reactor with separate feed of reactants I. Operation in absence of trans-membrane pressure gradients, Chem. Eng. Sci. 50 (1995) 2055.
[10] G. Saracco, J.W. Veldsink, G.F. Versteeg, W.P.M. van Swaaij, Catalytic combustion of propane in a membrane reactor with separate feed of reactants II. Operation in presence of trans-membrane pressure gradients, Chem. Eng. Sci. 50 (1995) 2833.
[11] G. Saracco, J.W. Veldsink, G.F. Versteeg, W.P.M. van Swaaij, Catalytic combustion of propane in a membrane reactor with separate feed of reactants III. Role of the catalyst load on reactor performance, Chem. Eng. Comm. 147 (1996) 29.
[12] H.W.J.P. Neomagus, W.P.M. van Swaaij, G.F. Versteeg, The catalytic partial oxidation of isobutene: operation in a fixed bed barrier reactor, in: Oral presentation at the III International Conference on Catalysis in Membrane Reactors, 8–10 September 1998, Copenhagen, Catal. Today, submitted for publication.
[13] E.A. Mason, A.P. Malinauskas, Gas transport in porous media: the Dusty-Gas-Model, in: Chemical Engineering Monographs, Vol. 17, Elsevier, Amsterdam, 1983.
[14] J.J. Spivey, Complete catalytic oxidation of volatile organics, Ind. Eng. Chem. Res. 26 (1987) 2165.
[15] R.B. Bird, W.E. Stewart, E.N. Lightfoot, Transport Phenomena, Wiley, New York, 1960.
[16] R.C. Reid, J.M. Prausnitz, B.E. Poling, The Properties of Gases and Liquids, IV Edition, McGraw-Hill, New York, 1987.
[17] V. Specchia, S. Sicardi, Conducibiltà assiale di calore in reattori catalitici a letto fisso, Atti Accad. Sci. Torino 114 (1980) 71 (in Italian).
[18] R.E. Lunberg, W.C. Reynolds, P.A. McCuen, Heat transfer in annular passages. Hydrodynamically developed laminar flow with arbitrarily prescribed wall temperatures or heat fluxes, Int. J. Heat Mass Trans. 6 (1963) 495.
[19] L. Montanaro, G. Saracco, Influence of some precursors on the physico-chemical characteristics of transition aluminas for the preparation of ceramic catalytic filters, Ceram. Inter. 21 (1995) 43.
[20] S.D. Jackson, J. Willis, G.D. McLellan, G. Webb, M.B.T. Keegan, R.B. Moyes, S. Simpson, P.B. Wells, R. Whyman, Supported metal catalysts: preparation, characterisation and function. I. Preparation and characterisation of platinum catalysts, J. Catal. 139 (1993) 191–206.
[21] J. Barbier, D. Bahloul, P. Marecot, Reduction of Pt/Al_2O_3 catalysts: effect of hydrogen and of water and hydrochloric acid vapor on the accessibility of platinum, J. Catal. 137 (1992) 377.
[22] W.D. Kingery, M.C. McQuarrie, Thermal conductivity: I. Concepts of measurement and factors affecting thermal conductivity of ceramic membranes, J. Am. Ceram. Soc. 37(2) (1954) 67.
[23] D. Peckner, I. Bernstein, Handbook of Stainless Steels, McGraw-Hill, New York, 1977.
[24] G. Saracco, G. Scibilia, A. Iannibello, G. Baldi, Methane combustion on Mg-doped $LaCrO_3$ perovskite catalysts, Appl. Catal. B: Environmental 8 (1996) 229.
[25] G. Saracco, L. Montanaro, Catalytic ceramic filters for flue gas cleaning. 1. Preparation and characterisation, Ind. Eng. Chem. Res. 34 (1995) 1471.
[26] R.W. Maatman, How to make a more effective platinum-alumina catalyst, Ind. Eng. Chem. 51 (1959) 913.
[27] R.W. Maatman, C.D. Prater, Adsorption and exclusion in the impregnation of porous catalytic supports, Ind. Eng. Chem. 49 (1957) 253.
[28] Y. Itaya, S. Maeda, M. Hasatani, Surface combustion of a pre-mixed methane-air gas on a porous ceramic, Int. Chem. Eng. 32(1) (1992) 123.
[29] A.L. Loeb, Thermal conductivity: VIII, A theory of thermal conductivity of porous materials, J. Am. Ceram. Soc. 37 (1954) 96.
[30] S. Sicardi, V. Specchia, F. Ferrero, A. Gianetto, Kinetics of combustion of methane with different catalysts, Atti Accad. Sci. Torino 116 (1982) 217.
[31] R.B. Anderson, K.C. Stein, J.J. Feenan, L.J.E. Hofer, Catalytic oxidation of methane, Ind. Eng. Chem. 53 (1961) 809.
[32] G. Saracco, V. Specchia, Catalytic ceramic filters for flue gas cleaning. 2. Catalytic performance and modeling thereof, Ind. Eng. Chem. Res. 34 (1995) 1480.